BULLETIN OF THE EARTHQUAKE
RESEARCH INSTITUTE
Vol. 55 (1980), pp. 369-385

18. Linear Transformation of Gravity Field and Terrestrial Heat Flow Assuming Steady-State Thermal Convection Currents.

By Yukio HAGIWARA,

Earthquake Research Institute, University of Tokyo

(Received May 20, 1980)

Abstract

The two-dimensional steady-state convection patterns are analytically obtained from the solutions of the equations of viscous fluid motion, continuity, thermal conduction and state. The emphasis is especially put on the derivation of convolution-type transformation formulas connecting gravity anomaly and horizontal fluid velocity with terrestrial heat flow. The simple frequency domain expressions in the Fourier transform can allow immediate recognition of the relationship between gravity anomaly and the other relevant quantities. The model calculations are made using values of the transformation formulas.

1. Introduction

The presence of convection currents in the earth's mantle can be supported from the simple premise that the solid mantle may behave as a fluid with respect to stress acting for a long term. The hypothesis that the horizontal motion of lithospheric plates is driven by the underlaid convection currents seems capable of explaining the global tectonic system that the plates are produced at mid-ocean ridges and move away toward deep-sea trenches. The high heat flow along mid-ocean ridges is presumably associated with up-coming fluid materials of the mantle heated below, and the low heat flow along trenches may be an indication of the down-going convection current.

If the thermal convection actually exists in the mantle, the gravity anomaly may reflect an effect of the convection-related density disturbance on the gravity field. A negative gravity anomaly is expected in high heat-flow regions because of low density related to the thermal expansion of the mantle material, while a down-going flow along subduc-

tion zones may possibly generate a positive gravity anomaly.

The gravity anomalies over mid-ocean ridges and deep-sea trenches have been discussed in relation to the mantle convection or the plate motion by many authors, whose papers have been reviewed (MCKENZIE *et al.*, 1974). The analytical treatments and the numerical experiments on simple two-dimensional models have been attempted to estimate steady-state or time-dependent behaviors of convection currents from the gravity field as well as terrestrial heat flow.

Our special interest is in the analytical method which describes the possible linear transformation of gravity field and terrestrial heat flow in the two-dimensional Cartesian coordinates, assuming the steady-state thermal convection of an incompressible Newtonian fluid of very high viscosity. The transformation formula can be obtained in the form of a convolution by taking the Fourier transforms of fluid velocity, gravity anomaly and terrestrial heat flow. The frequency domain representations enable us to solve the fluid dynamic equations in a much simpler expression which may allow immediate recognition of the relationship between convection currents and the relevant measurable quantities.

2. Formulation of Convection

The thermal convection of incompressible viscous fluid is governed by equations of fluid motion, continuity, thermal conduction and state. These equations can be expressed respectively as

$$\rho\frac{\mathrm{D}\boldsymbol{v}}{\mathrm{D}t}=-\mathrm{grad}\,p+\mu\nabla^2\boldsymbol{v}+\rho\boldsymbol{g}\,, \tag{1}$$

$$\mathrm{div}\,\boldsymbol{v}=0\,, \tag{2}$$

$$\frac{\mathrm{D}T}{\mathrm{D}t}=k\nabla^2T+A\,, \tag{3}$$

$$\rho=\rho_0(1-\alpha T)\,, \tag{4}$$

where ρ is the density, $\boldsymbol{v}$ the velocity vector, t the time, p the pressure, μ the coefficient of viscosity, $\boldsymbol{g}$ the gravity vector taken positive downward, T the temperature, k the thermal diffusivity, A the rate of internal heat generation, α the coefficient of thermal expansion, and $\mathrm{D}/\mathrm{D}t$ the Eulerian differential operator given by

$$\frac{\mathrm{D}}{\mathrm{D}t}=\frac{\partial}{\partial t}+(\boldsymbol{v}\,\mathrm{grad})\,.$$

To eliminate the non-linear terms snch as $(\boldsymbol{v}\,\mathrm{grad})\boldsymbol{v}$, we adopt here

the perturbation method in the slow motion approximation. ρ, p and T are divided into terms of basic state (denoted here by a bar) and of perturbation (denoted here by a prime) respectively, *i. e.*

$$\rho=\bar{\rho}+\rho'$$
$$p=\bar{p}+p'$$
$$T=\bar{T}+T'.$$

It is assumed that terms of the second and the higher power of $\boldsymbol{v}$, ρ' and p' are negligibly small as compared with the terms of basic state. Moreover, we assume the steady state of fluid motion and the rate of heat generation to be constant in the fluid. Then, (1), (3) and (4) can be rewritten in the forms of perturbation equations as followe:

$$\text{grad } p'=\mu\nabla^2\boldsymbol{v}+\rho\boldsymbol{g}, \tag{5}$$
$$\boldsymbol{v}\,\text{grad }\bar{T}=k\nabla^2T', \tag{6}$$
$$\rho'=-\alpha\rho_0T'. \tag{7}$$

In the two-dimensional Cartesian coordinates (x, z), in which z is taken downward, the above equations and (2) are expressed as

$$\frac{\partial p'}{\partial x}=\mu\nabla^2u, \tag{8}$$
$$\frac{\partial p'}{\partial z}=\mu\nabla^2w+\rho'g, \tag{9}$$
$$\frac{\partial u}{\partial x}+\frac{\partial w}{\partial z}=0, \tag{10}$$
$$u\frac{\partial\bar{T}}{\partial x}+w\frac{\partial\bar{T}}{\partial z}=k\nabla^2T', \tag{11}$$
$$\rho'=-\alpha\rho_0T', \tag{12}$$

where u and w are the velocity vector components in the x and y directions, respectively.

First of all, the fluid motion is described with a scalar function ψ called the stream function as

$$u=-\frac{\partial\psi}{\partial z},\qquad w=\frac{\partial\psi}{\partial x}. \tag{13}$$

We see that (13) satisfies the equation (10) of continuity. Moreover, we assume that $\bar{T}$ varies linearly at a constant rate with the depth, *i. e.*

$$\frac{\partial\bar{T}}{\partial x}=0,\qquad \frac{\partial\bar{T}}{\partial z}=\beta. \tag{14}$$

Substituting (13) and (14) into (8), (9), (11) and (12), we obtain

$$\mu\nabla^4\psi=-g\frac{\partial\rho'}{\partial x} \tag{15}$$

and

$$\nabla^6\psi=\frac{\alpha\beta\rho_0 g}{k\mu}\frac{\partial^2\psi}{\partial x^2} \tag{16}$$

In order to solve (16), the Fourier transform of ψ with respect to x is taken as

$$\psi^*(\xi, z)=\int_{-\infty}^{\infty}\psi(x, z)e^{-i\xi x}\mathrm{d}x\,. \tag{17}$$

Hereafter in this paper, the asterisk denotes a transformed function of ξ, the angular frequency having the dimension of a reciprocal length. The derivatives of ψ are transformed as

$$\int_{-\infty}^{\infty}\frac{\partial^2\psi}{\partial x^2}e^{-i\xi x}\mathrm{d}x=-\xi^2\psi^*$$

$$\int_{-\infty}^{\infty}\frac{\partial^4\psi}{\partial x^4}e^{-i\xi x}\mathrm{d}x=\xi^4\psi^*\,,$$

$$\int_{-\infty}^{\infty}\frac{\partial^6\psi}{\partial x^6}e^{-i\xi x}\mathrm{d}x=-\xi^6\psi^*\,,$$

so that the Fourier transform of (16) becomes

$$\frac{\mathrm{d}^6\psi^*}{\mathrm{d}z^6}-3\xi^2\frac{\mathrm{d}^4\psi^*}{\mathrm{d}z^4}+3\xi^4\frac{\mathrm{d}^2\psi^*}{\mathrm{d}z^2}+\xi^6(\lambda^3-1)\psi^*=0\,, \tag{18}$$

where

$$\lambda^3=\frac{\alpha\beta\rho_0 g}{k\mu\xi^4}=\frac{R}{D^4\xi^4} \tag{19}$$

with the Rayleigh number R, which is dimensionless. The convective motion appears when R takes an eigenvalue larger than the critical Rayleigh number.

The solution of (18) can easily be obtained in the form:

$$\begin{aligned}\psi^*=&C_1\cos(\xi z\sqrt{\lambda-1})+C_2\sin(\xi z\sqrt{\lambda-1})\\&+C_3\cos(\xi z\sqrt{\omega\lambda-1})+C_4\sin(\xi z\sqrt{\omega\lambda-1})\\&+C_5\cos(\xi z\sqrt{\omega^2\lambda-1})+C_6\sin(\xi z\sqrt{\omega^2\lambda-1})\end{aligned} \tag{20}$$

with six coefficients to be determined by boundary conditions. ω and ω^2 are solutions of a cubic equation $x^3-1=0$, which are

$$\omega=\frac{-1+\sqrt{3}\,i}{2}, \qquad \omega^2=\frac{-1-\sqrt{3}\,i}{2}. \tag{21}$$

The Fourier transform of the velocity field is described by using ψ^* in the form:

$$u^*=-\frac{\mathrm{d}\psi^*}{\mathrm{d}z}, \qquad w^*=i\xi\psi^*, \tag{22}$$

so that substitution of (20) into (22) gives us the solution of the velocity components.

Meanwhile, the Fourier-transformed expression of ρ' becomes

$$\begin{aligned}\rho^*=\frac{i\mu\xi^3\lambda^2}{g}\Big\{&C_1\cos(\xi z\sqrt{\lambda-1})+C_2\sin(\xi z\sqrt{\lambda-1})\\&+\omega^2C_3\cos(\xi z\sqrt{\omega\lambda-1})+\omega^2C_4\sin(\xi z\sqrt{\omega\lambda-1})\\&+\omega C_5\cos(\xi z\sqrt{\omega^2\lambda-1})+\omega C_6\sin(\xi z\sqrt{\omega^2\lambda-1})\Big\}.\end{aligned} \tag{23}$$

From (12), the temperature change is given in the Fourier transform as

$$T^*=-\frac{\rho^*}{\alpha\rho_0}. \tag{24}$$

3. Boundary Conditions

The convecting fluid is restricted to an infinite slab with a thickness of D, which is overlaid by a conducting layer with a thickness of H. The boundary conditions are given as follows: the temperature change is zero and the heat flow is given on the surface $z=-H$, the temperature change and the heat flow are continuous on the interface $z=0$, and the vertical fluid velocity and deviatoric shear stress are zero on both the surfaces $z=0$ and D. These are described in the forms:

$$\left.\begin{aligned}&T^*(\xi,-H)=0\\&Q^*(\xi,-H)=K_1\left[\frac{\mathrm{d}T^*}{\mathrm{d}z}\right]_{z=-H},\\&T^*(\xi,-0)=T^*(\xi,+0),\\&K_1\left[\frac{\mathrm{d}T^*}{\mathrm{d}z}\right]_{z=-0}=K\left[\frac{\mathrm{d}T^*}{\mathrm{d}z}\right]_{z=+0},\\&\psi^*(\xi,0)=\psi^*(\xi,D)=0,\\&\left[\frac{\mathrm{d}^2\psi^*}{\mathrm{d}z^2}\right]_{z=0}=\left[\frac{\mathrm{d}^2\psi^*}{\mathrm{d}z^2}\right]_{z=D}=0,\end{aligned}\right\} \tag{25}$$

where $Q^*(\xi, -H)$ is the Fourier transform of the heat flow given at $z=-H$, and K_1 and K are the thermal conductivities of the conducting layer and convecting one, respectively.

In the above, the shear stress condition is derived as follows: The shear stress

$$\tau=\mu\left(\frac{\partial u}{\partial z}+\frac{\partial w}{\partial x}\right)$$
$$=\mu\left(\frac{\partial^2\psi}{\partial z^2}-\frac{\partial^2\psi}{\partial x^2}\right)$$

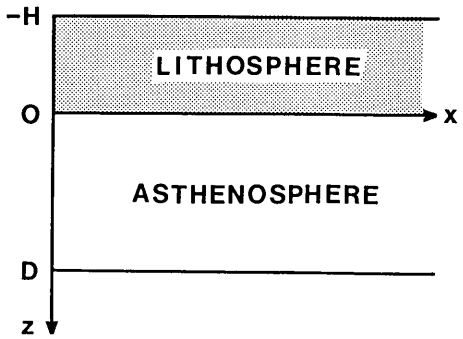

Fig. 1. Model structure used in this paper.

is transformed as

$$\tau^*=-\mu\left(\frac{\mathrm{d}^2\psi^*}{\mathrm{d}z^2}+\xi^2\psi^*\right),$$

so that the condition $\tau=0$ is equal to the last equation in (25) because of $\psi^*=0$.

In the superficial layer, only the equation of heat conduction is satisfied as

$$\nabla^2 T'=0, \tag{26}$$

the Fourier transform of which becomes

$$\frac{\mathrm{d}^2T^*}{\mathrm{d}z^2}-\xi^2T^*=0. \tag{27}$$

The solution of (27) satisfying the first and second conditions of (25) is then

$$T^*=\frac{Q^*(\xi, -H)}{K_1\xi}\sinh\{\xi(z+H)\}. \tag{28}$$

The six coefficients can be determined by using the last four conditions of (25) after a somewhat laborious algebra, *i. e.*

$$\left.\begin{aligned} C_1&=-\frac{\alpha\rho_0 g}{3i\mu K_1\xi^4\lambda^2}Q^*(\xi,-H)\sinh H\xi \\ C_3&=\omega C_1 \\ C_5&=\omega^2 C_1 \end{aligned}\right\} \tag{29}$$

$$\left.\begin{aligned} C_2&=-\frac{\alpha\rho_0 g}{i\mu K\xi^4\lambda^2}\frac{Q^*(\xi,-H)}{\sin(\xi D\sqrt{\lambda-1})}\left\{\frac{1}{M}\left(\cosh H\xi+\frac{KN}{3K_1}\sinh H\xi\right)\right. \\ &\qquad\left.-\frac{K}{3K_1}\sinh H\xi\cos(\xi D\sqrt{\lambda-1})\right\} \\ C_4&=-\frac{\alpha\rho_0 g}{i\mu K\xi^4\lambda^2}\frac{\omega Q^*(\xi,-H)}{\sin(\xi D\sqrt{\omega\lambda-1})}\left\{\frac{1}{M}\left(\cosh H\xi+\frac{KN}{3K_1}\sinh H\xi\right)\right. \\ &\qquad\left.-\frac{K}{3K_1}\sinh H\xi\cos(\xi D\sqrt{\omega\lambda-1})\right\} \\ C_6&=-\frac{\alpha\rho_0 g}{i\mu K\xi^4\lambda^2}\frac{\omega^2 Q^*(\xi,-H)}{\sin(\xi D\sqrt{\omega^2\lambda-1})}\left\{\frac{1}{M}\left(\cosh H\xi+\frac{KN}{3K_1}\sinh H\xi\right)\right. \\ &\qquad\left.-\frac{K}{3K_1}\sinh H\xi\cos(\xi D\sqrt{\omega^2\lambda-1})\right\} \end{aligned}\right\} \tag{29}'$$

where

$$\left.\begin{aligned} M&=\frac{\sqrt{\lambda-1}}{\sin(\xi D\sqrt{\lambda-1})}+\frac{\sqrt{\omega\lambda-1}}{\sin(\xi D\sqrt{\omega\lambda-1})}+\frac{\sqrt{\omega^2\lambda-1}}{\sin(\xi D\sqrt{\omega^2\lambda-1})} \\ N&=\frac{\sqrt{\lambda-1}}{\tan(\xi D\sqrt{\lambda-1})}+\frac{\sqrt{\omega\lambda-1}}{\tan(\xi D\sqrt{\omega\lambda-1})}+\frac{\sqrt{\omega^2\lambda-1}}{\tan(\xi D\sqrt{\omega^2\lambda-1})} \end{aligned}\right\} \tag{30}$$

Substitutions of the above-determined six coefficients into (20) and (23) give us the velocity field and the density disturbance, *i. e.* the temperature disturbance by (24), in the frequency domain expressions.

4. Velocity Field and Temperature Disturbance

The subject of this section is first to derive such transformation formulas as to connect the velocity field and the temperature disturbance with the terrestrial heat flow profile. Secondly, for actual calculations of the velocity field, the space domain formulas are derived by taking the inverse Fourier transforms of the relevant quantities.

The stream function and the temperature disturbance are expressed in the frequency domain as follows:

$$\phi^*(\xi,z)=\frac{\alpha\rho_0 g D^4}{i\mu K}E^*(\xi,z)Q^*(\xi,-H), \tag{31}$$

$$T^*(\xi, z)=\frac{D}{K}F^*(\xi, z)Q^*(\xi, -H)\,, \tag{32}$$

where

$$\begin{aligned}E^*(\xi, z)=-\frac{1}{\lambda^2\xi^4D^4}\Bigg[&\frac{1}{M}\left(\cosh H\xi+\frac{KN}{3K_1}\sinh H\xi\right)\\&\left\{\frac{\sin(\xi z\sqrt{\lambda-1})}{\sin(\xi D\sqrt{\lambda-1})}+\omega\frac{\sin(\xi z\sqrt{\omega\lambda-1})}{\sin(\xi D\sqrt{\omega\lambda-1})}+\omega^2\frac{\sin(\xi z\sqrt{\omega^2\lambda-1})}{\sin(\xi D\sqrt{\omega^2\lambda-1})}\right\}\\&-\frac{K}{3K_1}\sinh H\xi\left\{\frac{\sin(\xi(z-D)\sqrt{\lambda-1})}{\sin(\xi D\sqrt{\lambda-1})}\right.\\&\left.+\omega\frac{\sin(\xi(z-D)\sqrt{\omega\lambda-1})}{\sin(\xi D\sqrt{\omega\lambda-1})}+\omega^2\frac{\sin(\xi(z-D)\sqrt{\omega^2\lambda-1})}{\sin(\xi D\sqrt{\omega^2\lambda-1})}\right\}\Bigg]\end{aligned} \tag{33}$$

and

$$\begin{aligned}F^*(\xi, z)=\frac{1}{\xi D}\Bigg[&\frac{1}{M}\left(\cosh H\xi+\frac{KN}{3K_1}\sinh H\xi\right)\\&\left\{\frac{\sin(\xi z\sqrt{\lambda-1})}{\sin(\xi D\sqrt{\lambda-1})}+\frac{\sin(\xi z\sqrt{\omega\lambda-1})}{\sin(\xi D\sqrt{\omega\lambda-1})}+\frac{\sin(\xi z\sqrt{\omega^2\lambda-1})}{\sin(\xi D\sqrt{\omega^2\lambda-1})}\right\}\\&-\frac{K}{3K_1}\sinh H\xi\left\{\frac{\sin(\xi(z-D)\sqrt{\lambda-1})}{\sin(\xi D\sqrt{\lambda-1})}\right.\\&\left.+\frac{\sin(\xi(z-D)\sqrt{\omega\lambda-1})}{\sin(\xi D\sqrt{\omega\lambda-1})}+\frac{\sin(\xi(z-D)\sqrt{\omega^2\lambda-1})}{\sin(\xi D\sqrt{\omega^2\lambda-1})}\right\}\Bigg].\end{aligned} \tag{34}$$

In the special case of $\xi=0$, these two functions become

$$\left.\begin{aligned}E^*(0, z)&=0\\F^*(0, z)&=\frac{z}{D}-\frac{KH(z-D)}{K_1D^2}\end{aligned}\right\} \tag{35}$$

By taking the inverse Fourier transforms of (31) and (32), the space domain representations of them can be written in the convolution-type integrals:

$$\phi(x, z)=-\frac{\alpha\rho_0gD^4}{i\mu K}\int_{-\infty}^{\infty}E(x-x', z)Q(x', -H)\mathrm{d}x'\,, \tag{36}$$

$$T(x, z)=\frac{D}{K}\int_{-\infty}^{\infty}F(x-x', z)Q(x', -H)\mathrm{d}x'\,, \tag{37}$$

where $E(x, z)$ and $F(x, z)$, the inverse Fourier transforms of $E^*(\xi, z)$ and $F^*(\xi, z)$, are respectively

$$E(x,z)=\frac{1}{2\pi}\int_{-\infty}^{\infty}E^*(\xi,z)e^{i\xi x}\mathrm{d}\xi$$

$$=\frac{i}{\pi}\int_{-\infty}^{\infty}E^*(\xi,z)\sin\xi x\,\mathrm{d}\xi\,, \tag{38}$$

$$F(x,z)=\frac{1}{2\pi}\int_{-\infty}^{\infty}F^*(\xi,z)e^{i\xi x}\mathrm{d}\xi$$

$$=\frac{1}{\pi}\int_{-\infty}^{\infty}F^*(\xi,z)\cos\xi x\,\mathrm{d}\xi \tag{39}$$

For numerical calculations, by putting $x=ns$ in (n is the integer number, and s the spacing of digital data grid), (36) and (37) are rewritten in the digital forms:

$$\phi(n,z)=\frac{\alpha\rho_0 gD^1}{\mu K}\sum_{n'=-\infty}^{\infty}\phi(n-n',z)Q(n',-H)\,, \tag{40}$$

$$T(n,z)=\frac{D}{K}\sum_{n'=-\infty}^{\infty}\varphi(n-n',z)Q(n',-H)\,, \tag{41}$$

together with

$$\phi(n,z)=\frac{s}{i}E(n,z)=\frac{s}{\pi}\int_0^{\infty}E^*(\xi,z)\sin n\xi s\mathrm{d}\xi\,, \tag{42}$$

$$\varphi(n,z)=sF(n,z)=\frac{s}{\pi}\int_0^{\infty}F^*(\xi,z)\cos n\xi s\mathrm{d}\xi\,. \tag{43}$$

As the integrands of (42) and (43) diverge to infinity for high angular frequencies, we take a finite integral range within $\xi=\pi/s$. Such a truncation procedure is based on the premise that the digital sampling process with a spacing of s implies neglect of the frequency domain higher than π/s. In other words, the spatial distribution of angular frequencies higher than π/s is not dealt with in the digital process. Therefore, (42) and (43) can be respectively replaced by

$$\phi(n,z)=\frac{s}{\pi}\int_0^{\pi/s}E^*(\xi,z)\sin n\xi s\,\mathrm{d}\xi$$

$$=\int_0^1 E^*\left(\frac{\pi\xi'}{s},z\right)\sin n\pi\xi'\,\mathrm{d}\xi'\,, \tag{44}$$

$$\varphi(n,z)=\int_0^1 F^*\left(\frac{\pi\xi'}{s},z\right)\cos n\pi\xi'\,\mathrm{d}\xi'\,. \tag{45}$$

These two functions are numerically evaluated by taking the special cases of (35) into consideration.

5. Horizontal Fluid Velocity in the Upper Mantle

If the hypothesis that the convection drives the lithospheric plate motion is recognized, the laterally spreading speed of the plate must be closely related to the horizontal fluid velocity in the upper mantle layer. The stream function is fully determined on the basis of the preceding mathematical descriptions, so that the horizontal velocity on the boundary surface can be described in a linear transformation formula of the terrestrial heat flow on the outer surface.

The Fourier transform of the horizontal fluid velocity at $z=0$ is defined as

$$u^*(\xi, 0)=-\left[\frac{\mathrm{d}\psi^*}{\mathrm{d}z}\right]_{z=\ell}$$

$$=-\frac{\alpha\rho_0 gD^3}{i\mu K}U^*(\xi)Q^*(\xi, -H), \tag{46}$$

where

$$U^*(\xi)=D\left[\frac{\mathrm{d}E^*}{\mathrm{d}z}\right]_{z=0}$$

$$=-\frac{1}{\lambda^2\xi^3D^3}\left\{\frac{M'}{M}\left(\cosh H\xi+\frac{KN}{3K_1}\sinh H\xi\right)-\frac{KN'}{3K_1}\sinh H\xi\right\} \tag{47}$$

together with

$$\left.\begin{aligned} M'&=\frac{\sqrt{\lambda-1}}{\sin(\xi D\sqrt{\lambda-1})}+\frac{\omega\sqrt{\omega\lambda-1}}{\sin(\xi D\sqrt{\omega\lambda-1})}+\frac{\omega^2\sqrt{\omega^2\lambda-1}}{\sin(\xi D\sqrt{\omega^2\lambda-1})},\\ N'&=\frac{\sqrt{\lambda-1}}{\tan(\xi D\sqrt{\lambda-1})}+\frac{\omega\sqrt{\omega\lambda-1}}{\tan(\xi D\sqrt{\omega\lambda-1})}+\frac{\omega^2\sqrt{\omega^2\lambda-1}}{\tan(\xi D\sqrt{\omega^2\lambda-1})}. \end{aligned}\right\} \tag{48}$$

It can easily be proved that $U^*(\xi)$ is an odd function of ξ and $U^*(0)=0$.

Similarly to the treatments in the previous section, the space domain representation is given in the digital form:

$$u(n, 0)=-\frac{\alpha\rho_0 gD^3}{i\mu K}\sum_{n'=-\infty}^{\infty}\sigma(n-n')Q(n', -H) \tag{49}$$

where

$$\sigma(n)=sU(n)$$

$$=i\int_0^{\pi}U^*\left(\frac{\pi\xi'}{s}\right)\sin n\pi\xi'\,\mathrm{d}\xi'. \tag{50}$$

If the numerical values of the above integral are obtained, $u(x, 0)$ is obtained from a given profile of $Q(n, -H)$ using the relation (49). $\sigma(n)$ converges oscillatorily to zero with an increasing n.

6. Convection-Related Gravity Anomaly

The convection currents generate the density disturbance, which can be reflected on the gravity field. A negative gravity anomaly is expected in high heat-flow areas because of low density due to the thermal expansion of the mantle material, while a positive gravity anomaly is expected in high density but low heat-flow areas.

The gravity anomaly induced by the density change ρ' is expressed as

$$\Delta g(x, -H)=2G\int_{-\infty}^{\infty}\mathrm{d}x'\int_{0}^{D}\frac{z'+H}{(x'-x)^2+(z'+H)^2}\rho'(x', z')\mathrm{d}z', \tag{51}$$

where G is Newton's gravitational constant. The Fourier transform of (51) becomes

$$\Delta g^*(\xi, -H)=2\pi G\, e^{-H|\xi|}\int_{0}^{D}e^{-|\xi|z'}\rho^*(\xi, z')\mathrm{d}z'.$$

A somewhat complicated performance of the above integration results in

$$\Delta g^*(\xi, -H)=\frac{2\pi G\alpha\rho_0 D^2}{K}\Gamma^*(\xi)Q^*(\xi, -H) \tag{52}$$

where

$$\Gamma^*(\xi)=-\frac{1}{\xi^2D^2\lambda}\frac{e^{-H|\xi|}}{M}\Big[\cosh H\xi\cdot(M''-N''e^{-D|\xi|}) -\frac{K}{3K_1}\sinh H\xi\cdot\{MN''-NM''-e^{-D|\xi|}(MM''-NN'')\}\Big] \tag{53}$$

together with

$$\left.\begin{aligned}M''&=\frac{\sqrt{\lambda-1}}{\sin(\xi D\sqrt{\lambda-1})}+\frac{\omega^2\sqrt{\omega\lambda-1}}{\sin(\xi D\sqrt{\omega\lambda-1})}+\frac{\omega\sqrt{\omega^2\lambda-1}}{\sin(\xi D\sqrt{\omega^2\lambda-1})}\\ N''&=\frac{\sqrt{\lambda-1}}{\tan(\xi D\sqrt{\lambda-1})}+\frac{\omega^2\sqrt{\omega\lambda-1}}{\tan(\xi D\sqrt{\omega\lambda-1})}+\frac{\omega\sqrt{\omega^2\lambda-1}}{\tan(\xi D\sqrt{\omega^2\lambda-1})}\end{aligned}\right\} \tag{54}$$

In the special case of $\xi=0$, we can easily prove

$$\Gamma^*(0)=-\frac{1}{2}\left(1+\frac{2KH}{K_1D}\right). \tag{55}$$

Similarly to the mathematical procedures in the previous sections, the digital form of the inverse transform of (52) can be described as

$$\Delta g(n, -H)=\frac{2\pi G\alpha\rho_0 D^2}{K}\sum_{n'=-\infty}^{\infty}\gamma(n-n')Q(n', -H) \tag{56}$$

where

$$\gamma(n)=s\Gamma(n)$$
$$=\int_0^1 \Gamma^*\left(\frac{\pi\xi'}{s}\right)\cos n\pi\xi'\,\mathrm{d}\xi'\,. \tag{57}$$

$\gamma(n)$ converges oscillatorily to zero with an increasing n. If $\gamma(n)$ is numerically evaluated, Δg can be obtained from given data of Q by summing up the terms of (56).

7. Model Calculations

The upper-mantle structure is known to some extent on the basis of the observations of seismic wave propagation and attenuation and high-pressure experiments of mantle-forming ultrabasic materials. Although our present knowledge is restricted, the asthenosphere is presumed to be a layer of about 200 km thick below a 100 km thick lithospheric plate. The existence of a low-velocity layer and the S-wave attenuation may possibly indicate that the asthenosphere is partially melted, in other words, a fluid in a general sense. The vertical motion due to the isostatic recovery of an asthenosphere below a lithospheric plate loaded by ice estimates the coefficient of viscosity to be 10^{19} N sec/m^2.

The laterally spreading speed of the ocean floor is thought to be 3 to 10 cm/year by the Vine and Matthews hypothesis (VINE and MATTHEWS, 1963) of geomagnetic lineations parallel to ocean ridges. The horizontal fluid velocity in the upper asthenosphere may be of the same order as that of the ocean-floor spreading motion. On the other hand, the horizontal motion of the plate compresses the island-arc crust at a rate of a few cm/year, which is actually observed by repeated trilateration surveys. The down-going plate-driving convection speed under an ocean trench may be closely related to the crustal compression rate.

Based on the above geophysical grounds, the model structure used in this paper consists of two layers as shown in Fig. 1. The upper layer is a thermally conductive infinite slab which has a thickness of 100 km. The thickness of the convective underlayer is a variable less than several hundred kilometers. The other parameters are chosen as $\alpha=3\times10^{-5}$ deg^{-1}, $\beta=2\times10^{-5}$ deg/km, $\rho_0=3.5$ g/cm^3, $k=4\times10^{-2}$ cm^2/sec and $K_1=K=4\times10^{-2}$ cal cm^{-1}sec^{-1}deg^{-1}. The coefficient of viscosity is determined by (19)

$$\mu=\frac{\alpha\beta\rho_0 gD^4}{kR} \tag{58}$$

from the Rayleigh number assumed to be 10^3, 10^4 and 10^5.

In the present calculation method, an arbitrary profile of terrestrial

heat flow can be applied as an input to (49) and (56) for respectively obtaining the horizontal fluid velocity at the plate-fluid boundary and the gravity anomaly distribution over the surface. For simplicity, the first model has a symmetric profile of heat-flow anomaly as indicated at the top of Fig. 2. The maximum heat flow anomaly amounts to 1 HFU (heat flow unit$=10^{-6}$ cal cm^{-2}sec^{-1}). The corresponding convection flow and temperature distribution of a fluid with the Rayleigh number $R=10^4$ in a 200 km thick underlayer results in a horizontal fluid velocity amounting to a few cm/year and about an -80 mgal gravity low. The obtained velocity range agrees well with both the geophysically estimated ocean-floor spreading motion and the crustal strain accumulation rate. The amount of gravity low is also comparable with the values observed over the Mid-Atlantic Ridge (TALWANI and LEPICHON, 1969).

When a heat-flow input similar to Fig. 2 is applied to the $R=10^5$ fluid under the same conditions as above, the output velocity becomes much larger (see Fig. 3). The minimum value of gravity anomaly increases slightly to -60 mgal. The upper convection cell is somewhat prolonged in shape. In addition, an inversely rolling cell appears newly in the bottom of the layer. The associated isothermal flux forms a hot spot in the upper part of the convection layer and a low temperature zone below the hot spot. The location of the hot spot rises up as compared with that in Fig. 2a.

The numerical calculation of the horizontal fluid velocity at $x=200$ km on the plate-fluid boundary results in the relationship against the thickness of an underlayer as shown in Fig. 4a. Despite of changes in the Rayleigh number, the velocity range seems to be consistent with the actual plate motion. Fig. 4b shows the gravity anomaly versus the thickness of a convection layer. The long-wavelength topography of an ocean ridge can be isostatically maintained by the mass deficiency due to the thermal expansion. The convection-related negative gravity anomalies exceeding -100 mgal or so can be partially compensated for by the topographic effects, so that the free-air anomaly expected over ocean ridges may be as large as several -10 mgal. Fig. 4c shows the relation between the coefficient of viscosity, calculated from (58), and the thickness of a convection layer together with parameters of the Rayleigh number. The order of the obtained coefficient seems to be plausible.

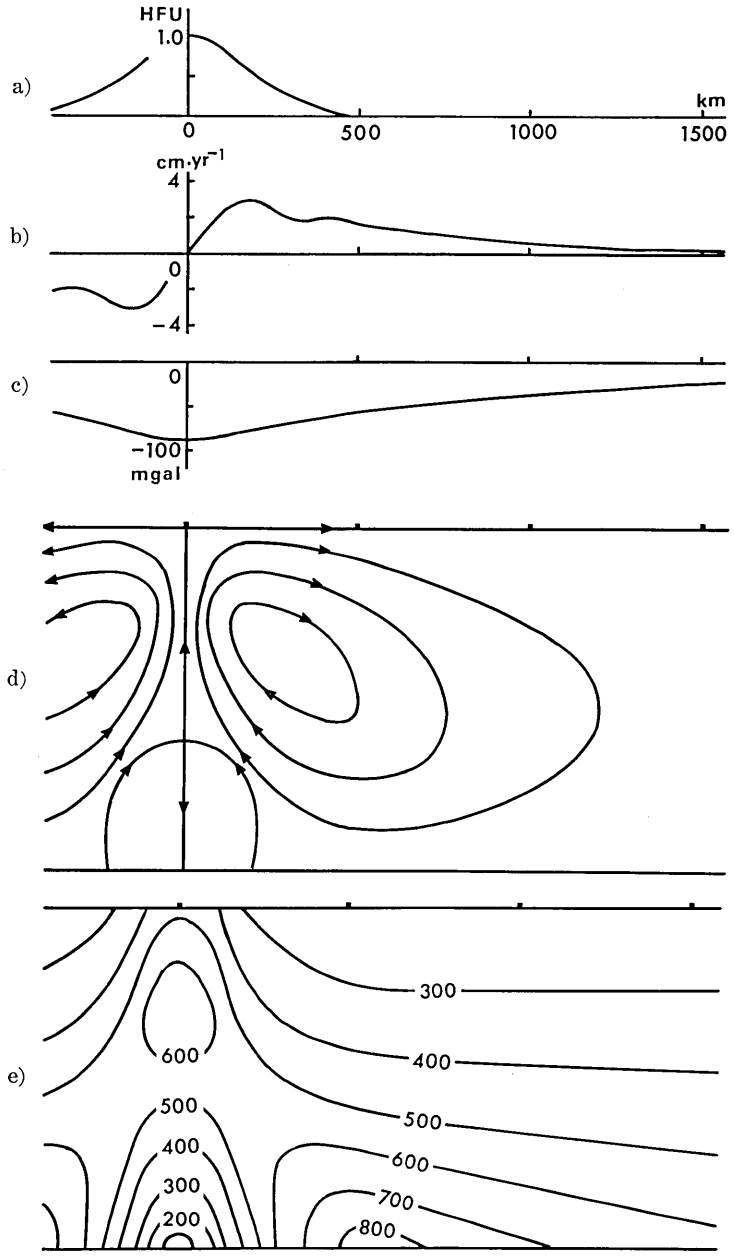

Fig. 2. Convection model ($H=100$ km, $D=200$ km, $R=10^4$).
a) Given heat flow profile.
b) Horizontal fluid velocity at the plate-fluid boundary.
c) Convection-related gravity anomaly.
d) Stream function. Contour interval is 0.1 cm²/sec.
e) Isothermal flux in °C.

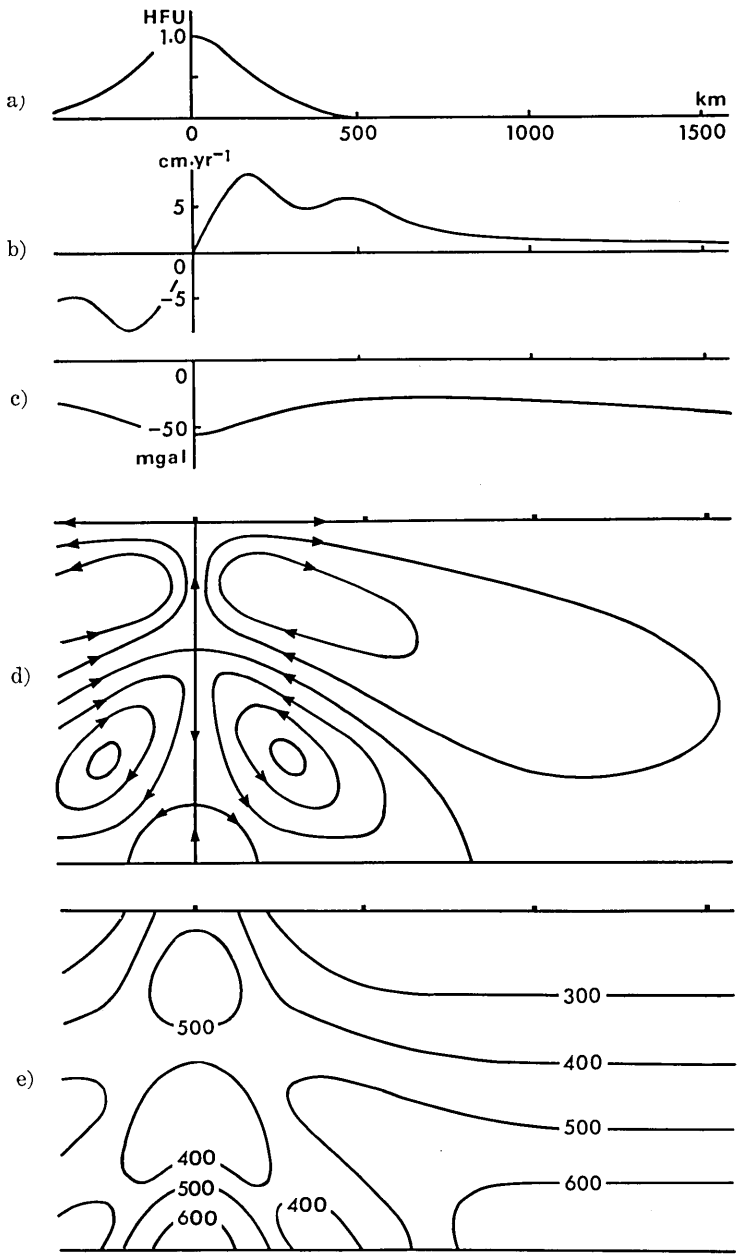

Fig. 3. Convection model ($H=100$ km, $D=200$ km, $R=10^5$).
a) Given heat flow profile.
b) Horizontal fluid velocity at the plate-fluid boundary.
c) Convection-related gravity anomaly.
d) Stream function. Contour interval is 0.2 cm²/sec.
e) Isothermal flux in °C.

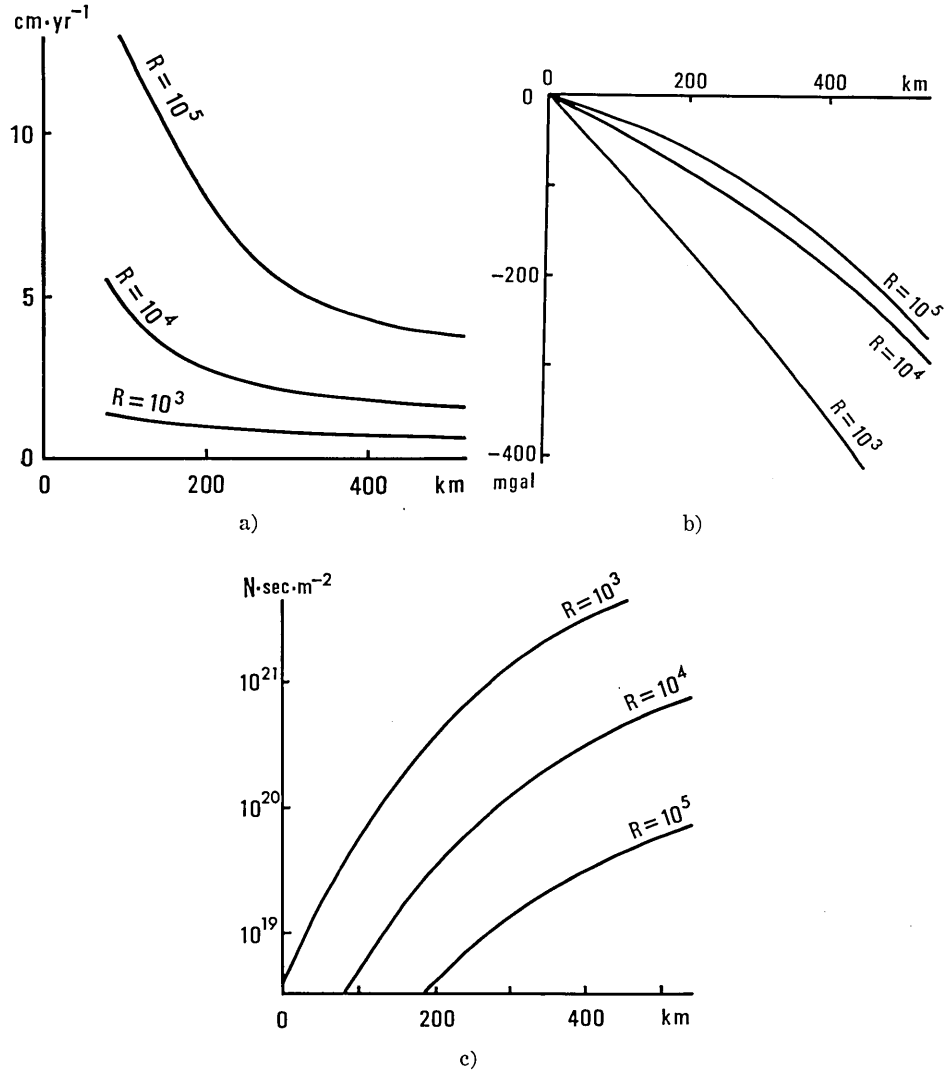

Fig. 4. a) Horizontal fiuid velocity at $x=200$ km on the plate-fiuid boundary versus the thickness of a convection layer.
b) Convection-related gravity anomaly versus the thickness of a convection layer.
c) Coefficient of viscosity versus the thickness of a convection layer.

8. Conclusion

The numerical experiments of a convection show that the convection pattern sometimes becomes unstable in a large Rayleigh number. In some cases, the instability is caused by errors due to numerical treat-

ments using finite-difference techniques. For the purpose of overcoming such an instability, we should use simple mathematical expressions connecting convection flows with measurable quantities such as heat flow, gravity anomaly and horizontal fluid velocity at the plate-fluid boundary.

This paper describes the linear transformation formulas convenient for actual computations in which the gravity anomaly and the horizontal fluid velocity at the plate-fluid boundary can be estmated from a given profile of heat flow. The associated convection flow and isothermal flux can also be obtained by using similar transformation formulas.

The model structure consists of a convecting layer between the shear stress-free boundaries overlaid by a 100 km thick lithospheric plate. The results of model calculations of high heat-flow over an ocean ridge agree well with geophysical observations. The present method, however, fails in obtaining a plausible streamline pattern which corresponds to the subduction zone obliquely thrusting down to the bottom of an island-arc structure. The assumption of uniform physical parameters throughout the convection layer may not be appropriate for realizing a subduction system.

References

McKenzie, D.P., J.M. Roberts and N.O. Weiss, Convection in the earth's mantle: towards a numerical simulation, *J. Fluid Mech.*, **62**, 465-538, 1974.

Talwani, M. and X. LePichon, Gravity field over the Atlantic Ocean. In the Earth's Crust and Upper Mantle (Ed. P.J. Hart), p. 341. Am. Geophys. Union Monograph 13.

Vine, F.J. and D.H. Matthews, Magnetic anomalies over oceanic ridges, *Nature*, **199**, 947-949, 1963.

---

18. 定常熱対流を仮定した重力と熱流量の線形変換

地震研究所　萩原幸男

2 次元定常熱対流を仮定したとき，熱流量を入力として重力と表層における水平方向の流速を出力とするようなフーリエ積分変換式を提示する。この変換式を用いて，簡単なモデル熱流量分布が与えられたとき，海嶺上の流れ関数と温度分布，重力異常と表層の水平流速を計算する。